Control of crystal polarity in a wurtzite crystal: ZnO films grown by plasma-assisted molecular-beam epitaxy on GaN

Soon-Ku Hong,* Takashi Hanada, Hang-Ju Ko, Yefan Chen, and Takafumi Yao
Institute for Materials Research, Tohoku University, Sendai 980-8577, Japan

Daisuke Imai, Kiyoaki Araki, and Makoto Shinohara
Surface Analysis and Semiconductor Equipment Division, Shimadzu Co., Kanagawa 259-1304, Japan

Koh Saitoh and Masami Terauchi
Institute for Multidisciplinary Research of Advanced Materials, Tohoku University, Sendai 980-8577, Japan
(Received 26 July 2001; revised manuscript received 14 December 2001; published 8 March 2002)

ZnO/GaN heterointerfaces are engineered to control the polarity of ZnO films grown by plasma-assisted molecular beam epitaxy on Ga-polar GaN templates. The polarity of ZnO films is determined both by coaxial impact collision ion scattering spectroscopy (CAICISS) and by convergent beam electron diffraction (CBED). Polarity inversion can be achieved by inserting an interface layer with a center of symmetry, because the polarity comes from a lack of the center of symmetry. An O-polar (anion-polar) ZnO film can be grown on Ga-polar (cation-polar) GaN by inserting a Ga_2O_3 layer at the interface, while Zn-polar ZnO is grown on GaN without forming an interface layer. A single-crystalline monoclinic Ga_2O_3 layer, which has a center of symmetry, is formed by O-plasma preexposure on the Ga-polar GaN surface prior to ZnO growth, while the ZnO/GaN interface without any extra layer is formed by Zn preexposure. The orientation relationship between ZnO, Ga_2O_3, and GaN is determined as $[2\text{-}1\text{-}10]_{ZnO} \| [010]_{Ga_2O_3} \| [2\text{-}1\text{-}10]_{GaN}$ and $(0001)_{ZnO} \| (001)_{Ga_2O_3} \| (0001)_{GaN}$. The CAICISS results reveal the growth of an O-polar ZnO film on O-plasma-preexposed GaN, while a Zn-polar ZnO film on Zn-preexposed GaN. The origin of the observed features in polar-angle-dependent CAICISS spectra can be analyzed by considering the shadow cones of Zn and O atoms formed by incident ions and shadowing and focusing effects of scattered ions. Azimuthal-angle-dependent CAICISS spectra reveal the surfaces of both Zn- and O-polar ZnO films as mixture of c and $c/2$ planes with a ratio of about 50:50. The ZnO film with a Ga_2O_3 interface layer shows a degradation in the crystal quality as evidenced by a broadening of the x-ray rocking curves. The CBED results for the O-plasma-preexposed samples reveal Ga-polar GaN and O-polar ZnO for the O-plasma-preexposed samples, which directly confirms polarity inversion from cation to anion polar. On the other hand, Zn-polar ZnO CBED patterns are obtained from ZnO films grown on Zn-preexposed Ga-polar GaN, which indicates the same cation polarity for a ZnO/GaN interface without the formation of an interface layer. It is noted that no planar or faceted inversion domain boundaries are formed to invert the polarity (from Ga polar to O polar). This indicates that we can control the polarity by engineering interfaces.

DOI: 10.1103/PhysRevB.65.115331 PACS number(s): 68.35.Fx, 81.05.Dz, 68.35.Ct

I. INTRODUCTION

A recent investigation of ZnO has revealed that this material is promising for exciton-based photonic devices in the ultraviolet region.[1–3] High-quality ZnO films have been successfully grown both on Al_2O_3 substrates[4,5] and on GaN/Al_2O_3 templates[6] by plasma-assisted molecular beam epitaxy (P-MBE). Those high-quality ZnO films are grown with the growth direction parallel to the c axis, which inevitably results in either Zn- or O-polar films. As has been demonstrated in the case of GaN epitaxy,[7–10] the lattice polarity of a wurtzite-structure film has crucial effects on growth processes, material properties, and impurity doping. It is reported that the growth mechanism, surface morphology, and structural properties of ZnO layers show considerable difference between homoepitaxial growths on Zn- and O-polar surfaces.[11]

Very recently we have reported success in controlling the growth of Zn- and O-polar ZnO films on GaN templates by changing the pregrowth treatments.[12] Since the GaN template grown by metal organic chemical vapor deposition (MOCVD) has Ga-polar nature as evidenced by coaxial impact collision ion scattering spectroscopy (CAICISS), the growth of ZnO without causing oxidation would result in Zn-polar layers. Hence Zn pretreatment has been adopted to protect oxidation and thereby helps grow Zn-polar ZnO layers. In order to invert polarity from a cation-polar to an anion-polar surface, a Ga_2O_3 interface layer, which was formed by oxidizing Ga-polar GaN templates with O plasma, has been inserted in between the ZnO layer and the GaN template. Since Ga_2O_3 has inversion symmetry with O surfaces both at the top and bottom, the resultant ZnO layers should show O polarity. The polarity of the ZnO films has been confirmed by CAICISS (Ref. 12) and convergent beam electron diffraction (CBED). We would like to note, however, that lattice polarity is different from surface termination. Lattice polarity is a bulk property as determined by the bond sequence in the crystal, while surface termination by atoms terminating the surface. Consequently, there are four types of wurtzite ZnO {0001} surface structures as schemati-

 ©2002 The American Physical Society

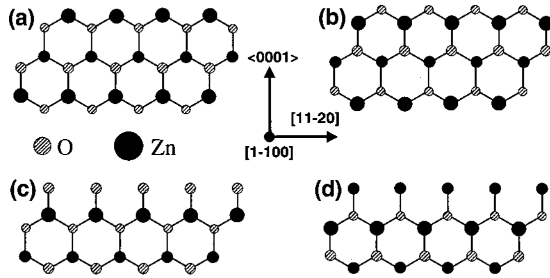

FIG. 1. Four kinds of wurtzite-structure {0001} ZnO surfaces: (a) Zn-polar surface with Zn-atom termination, (b) O-polar surface with Zn-atom termination, (c) Zn-polar surface with O-atom termination, and (d) O-polar surface with Zn-atom termination.

cally shown in Fig. 1: (1) Zn-polar surface with Zn-atom termination [Fig. 1(a)], (2) Zn-polar surface with O-atom termination [Fig. 1(c)], (3) O-polar surface with O-atom termination [Fig. 1(b)], and (4) O-polar surface with Zn-atom termination [Fig. 1(d)]. Detailed analysis is needed to determine both the lattice polarity and the surface termination of the ZnO films. Additionally, the effect of lattice polarity on growth processes and the materials properties of ZnO layers have not been fully addressed yet.

The purposes of this article are to perform detailed analysis of the structure of ZnO films grown on GaN templates with different pregrowth treatments and to discuss the effects on lattice polarity and structural properties.

II. PREGROWTH TREATMENTS AND MBE GROWTH

We used 4-μm-thick Ga-polar GaN epilayers grown by MOCVD on (0001) Al_2O_3 as templates for ZnO epitaxy. The GaN template was thermally cleaned at 700–750 °C in ultrahigh vacuum for about 1 h after being decreased in acetone and methanol. The reflection high-energy electron diffraction (RHEED) pattern from the GaN surface showed a streaky feature after this procedure indicative of a cleaned GaN surface.

Since the substrates used in this study is of Ga-polar GaN (cation-polar), the growth of Zn-polar ZnO films would be possible if we could form "N-Ga-O-Zn" bonding at the interface. However, the formation of such an interface would not be so easy because of the high reactivity of Ga with oxygen, which leads to the formation of an oxide layer at the interface during the initial growth of ZnO.[13] Therefore, in order to form "N-Ga-O-Zn" bonding at the interface and to grow Zn-polar ZnO films on Ga-polar GaN, Zn preexposure was adopted, which may prevent preferential reaction of a Ga-polar GaN surface with energetic O plasma. In order to convert the bond sequence, a Ga_2O_3 interface layer was formed by oxidizing the GaN surface prior to ZnO epitaxy.

Two types of pregrowth treatments were examined in order to control the interface bonding between the ZnO epilayer and GaN template: (1) Zn preexposure for 2–3 min to achieve Zn-polar growth and (2) O-plasma preexposure for 3–5 min to form a Ga_2O_3 interface layer, which should lead to O-polar ZnO growth on the Ga-polar GaN template. The Zn or O-plasma preexposure was carried out at 700 °C, in which a conventional *K* cell and a radio frequency (rf) oxygen plasma were used as zinc and oxygen sources, respectively. We have also tried prolonged oxygen exposure for 20 min to investigate the effects of overexposure of oxygen plasma on the oxidized surface layer and the growth process of ZnO.

ZnO films were grown at 700 °C directly on the GaN templates without depositing low-temperature buffer layers to investigate the effects of the surface polarity of GaN templates on the growth processes and material properties, although the crystal quality of ZnO epilayers had been greatly improved by depositing low-temperature ZnO buffer layers at 300 °C on GaN templates.[14] We have confirmed that for the lattice polarity of ZnO layers therefore the interface structure has been basically determined by the pretreatments of GaN templates not by the growth conditions of ZnO at least under the growth conditions we have examined. In the ZnO growth, Zn flux was set to about 0.15–0.20 nm/sec, which was monitored by a quartz thickness monitor before and after growth. O-plasma conditions were set to 400 W of power with an oxygen gas flow rate of 3.5 SCCM (SCCM denotes cubic centimeter per minute at STP). Growth conditions with such a flux ratio were oxygen rich and typical working pressure was 9×10^{-5} Torr. The thickness of ZnO films was about 150 nm.

As expected, RHEED did not show any appreciable change by Zn exposure, which indicates a small adsorption of Zn as is the case of Zn adsorption onto a GaAs surface.[15] Nevertheless, the Zn preexposure protected from selenidation of a GaAs substrate surface during ZnSe epitaxy.[15] Similarly, the GaN template surface did not show any trace of oxidation in terms of transmission electron microscopy (TEM) investigation as will be discussed later, although the growth of ZnO starts with impinging O plasma onto the GaN substrate, while Zn had been kept exposed. RHEED showed only a slight change from the streaky pattern of a GaN clean surface at the very beginning of ZnO epitaxy, which supports the TEM investigation. As the growth proceeded, however, the streaky RHEED pattern turned into a spotty one due to the onset of three-dimensional growth triggered presumably by the generation of misfit dislocations.[16] We would like to note that the critical thickness for the generation of misfit dislocations is estimated to be about 7 nm for ZnO growth on GaN.[16]

On exposing oxygen plasma onto a cleaned GaN surface without Zn preexposure, however, the RHEED pattern showed an appreciable change from streaky to diffusive due to the onset of oxidation. The growth of ZnO started with impinging Zn, while the oxygen plasma was kept on. The RHEED initially showed diffused streaks and gradually changed into a spotty pattern indicating three-dimensional growth. As the preexposure time of oxygen plasma was prolonged, the RHEED became more diffusive. With a prolonged preexposure of oxygen plasma longer than 15 min, diffraction spots eventually disappeared, indicating the formation of amorphous layers at least at the surface. The RHEED pattern showed essentially the same features even after annealing at higher temperature of 760 °C and for a longer time of 4 h under UHV. By depositing 20-nm-thick

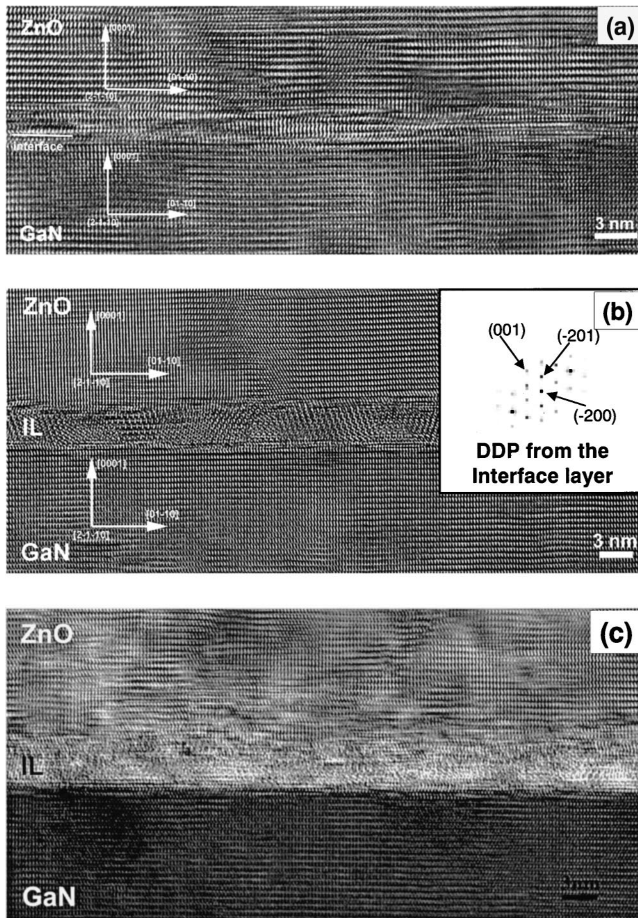

FIG. 2. HRTEM micrographs showing ZnO films on Ga-polar GaN templates with (a) Zn preexposure, (b) O-plasma preexposure, and (c) prolonged O-plasma preexposure. The inset in (b) shows a diffraction pattern obtained from the interface layer.

ZnO on the amorphous layers, a weak-diffusive ring RHEED pattern appeared. As the growth proceeded, the ring RHEED pattern gradually evolved into a spotty one. With the deposition of a ZnO layer thicker than 50 nm, the RHEED pattern completely changed to a spotty one. The observed evolution of the RHEED pattern showed a structural change from amorphous to single crystalline via a polycrystalline phase.

III. INTERFACE STRUCTURE ANALYSIS BY TEM

The interface structure of the ZnO/GaN heteroepitaxial layers has been investigated by high-resolution transmission electron microscopy (HRTEM). The interface structure showed drastic difference between the Zn preexposure and O-plasma preexposures. No interface layer was formed in between the GaN template and ZnO overlayer in the case of Zn preexposure [Fig. 2(a)], while an interface layer was observed for the O-plasma preexposure case [Figs. 2(b) and 2(c)]. Figure 2(b) shows a cross-sectional HRTEM micrograph of a ZnO/GaN interface with O-plasma preexposure for 3 min. The interface layer thickness measures 3.5 nm. As indicated by the Fourier transform of the interface layer image shown in the inset, the interface layer is single

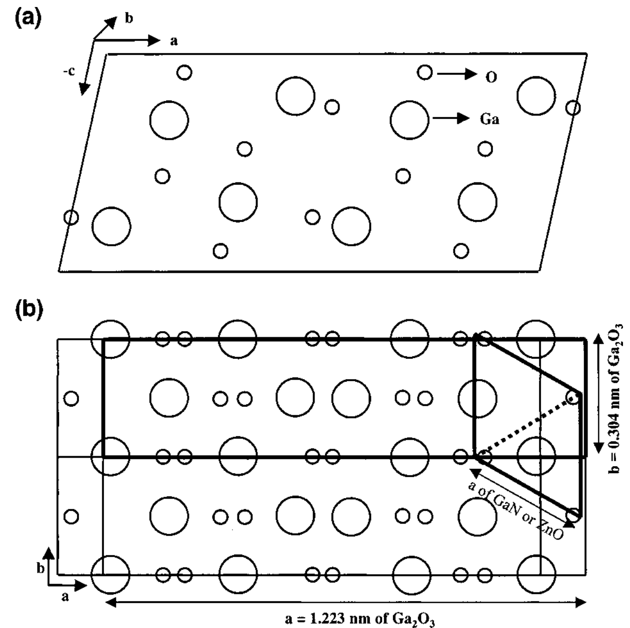

FIG. 3. (a) Ga_2O_3 unit cell viewed along the [010] direction. (b) schematic diagram showing presumable in-plane lattice matching where the Ga_2O_3 unit cell and hexagonal unit of GaN (or ZnO) are overlapped.

crystalline. The distances between the diffraction planes marked by the arrows are 0.52 ± 0.01, 0.53 ± 0.01, and 0.47 ±0.01 nm. These interplane spacings can be assigned to the (001), (-200), and (-201) diffraction planes of monoclinic Ga_2O_3 and the zone axis can be assigned to [010]. Detailed analysis of the interface layer suggested that the interface layer was indeed of Ga_2O_3.[17] The orientation relationship between ZnO, Ga_2O_3, and GaN would be $[2\text{-}1\text{-}10]_{ZnO}\|[010]_{Ga_2O_3}\|[2\text{-}1\text{-}10]_{GaN}$ and $(0001)_{ZnO}\|(001)_{Ga_2O_3}\|(0001)_{GaN}$. It is noted that both interfaces of ZnO/Ga_2O_3 and Ga_2O_3/GaN are sharp with small interface fluctuation. In the case of prolonged O-plasma preexposure [Fig. 2(c)], the interface of ZnO/Ga_2O_3 shows a large fluctuation as compared to the Ga_2O_3/GaN interface, although the thickness of the Ga_2O_3 interface layer is about 3.5 nm as well.

We have further investigated possible in-plane atomic arrangements at the interface based on the observed orientation relationship using the unit cells of bulk Ga_2O_3, GaN, and ZnO. Figure 3(a) shows a Ga_2O_3 unit cell viewed along the [010] direction. A unit cell of Ga_2O_3 contains 8 Ga and 12 O atoms and 10 fractional planes along the *c* direction. Figure 3(b) shows a projection view of two Ga_2O_3 unit cells along the direction normal to the (001) plane, in which one hexagonal unit cell of GaN (or ZnO) is overlapped onto a Ga_2O_3 unit cell in accordance with the observed orientation relationship. In this schematic diagram, we have not considered the in-plane or out-of-plane rearrangement of atoms at the interface. Although the lattice constant of Ga_2O_3 along the [010] direction (0.304 nm) is slightly smaller than the in-plane lattice constants of GaN (0.319 nm) and ZnO (0.325 nm), the lattice constant of Ga_2O_3 along the [100] direction

(1.223 nm) is about 4 times larger than the corresponding lattice parameters of GaN and ZnO. Because of such a large difference in the lattice constant between Ga_2O_3 and ZnO (or GaN), one-to-one direct matching of the three unit cells is impossible. Instead, lattice matching of one unit of Ga_2O_3 along the [100] direction and four unit cells of GaN or ZnO along the [01-10] direction is possible considering domain matching epitaxy.[18] This situation may facilitate the epitaxial growth of single-crystalline ZnO in spite of the large lattice misfit with the Ga_2O_3 interface layer. Thus the lattice misfits along the [010] ($b=0.304$ nm) and [100] ($a=1.223$ nm) axes of Ga_2O_3 with the [2-1-10] ($a=0.319$ nm) and [01-10] ($4\sqrt{3}a/2=1.105$ nm) directions of GaN are reduced to −4.7% and 10.7%, respectively. The corresponding lattice misfits between Ga_2O_3 and ZnO are −6.5% and 8.6%, respectively.

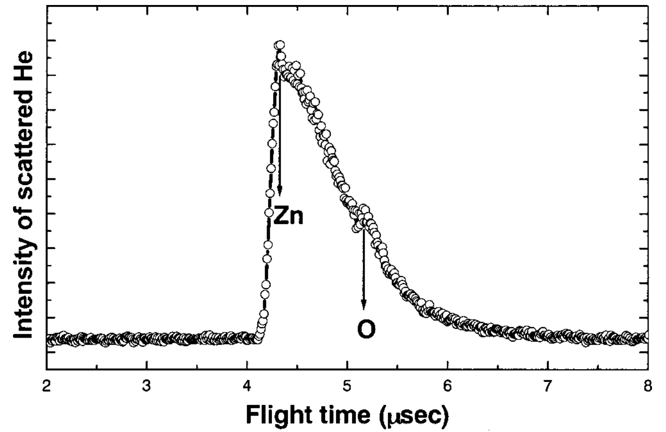

FIG. 4. TOF spectrum obtained from the ZnO film.

IV. SURFACE STRUCTURE ANALYSIS BY CAICISS

CAICISS is low-energy ion scattering spectroscopy with an incident beam energy at a few keV and has been frequently used to determine the lattice polarity of crystals.[19–22] Compared with Rutherford backscattering spectroscopy (RBS) with a few MeV ions, the diameter of a shadow cone (or a blocking cone) is large due to the significant screening effect of electrons in low-energy ion scattering.[23] Therefore, the shadowing effect (i.e., the formation of shadow cones) by incident ions, the blocking effect (i.e., the formation of blocking cones) by scattered ions, and the focusing effect (i.e., the focusing of ion flux at the edge of a cone) have important influences on the CAICISS spectra, which makes this technique surface sensitive. Since the experimental scattering angle of CAICISS is nearly 180° due to coaxial backscattering, it is possible to understand the features observed in a CAICISS spectrum based on a simple geometrical consideration of the surface structure, taking the shadowing effect by incident ions and the focusing effect by scattered ions into account.

A. Time-of-flight spectrum from the ZnO film

Primary He^+ ions with an energy of 2 keV were used for CAICISS measurements (Shimadzu Co., TALIS 9700). CAICISS signal intensities were measured either by varying the incident angle with its azimuthal direction along [11-20] or by varying the azimuth angle around the ⟨0001⟩ direction with an incident angle of 58.5°. After installing a sample into the CAICISS chamber, the sample was heated at 200 °C for 30 min to remove contamination from the sample surface.

Figure 4 shows a typical time-of-flight (TOF) CAICISS spectrum from a ZnO film. The total time of flight T_t $(=T_1+T_2)$ can be expressed as follows:

$$T_t=T_1+T_2=\frac{L_1}{v_1}+\frac{L_2}{v_2}=\frac{L_1}{v_1}+\frac{L_2}{v_1}\left(\frac{M+m}{M-m}\right). \quad (1)$$

Here L_1, T_1, and v_1 are distances from the ion source to the sample surface, the time of flight, and the velocity of the incident ion, respectively. L_2, T_1, and v_1 are the distances from the sample surface to the mass analyzer, the time of flight, and the velocity of backscattered ions, respectively. Remembering that $mV_1{}^2/2=qV$, where q is the electronic charge and V is the acceleration voltage of 2 keV in the present measurements, the total times of flight for a He^+ ion scattered by Zn and O atoms are estimated to be 4.3 and 5.2 μsec, respectively. The observed sharp peak at 4.3 μsec and the shoulder at 5.2 μsec in Fig. 4 correspond to backscattered He^+ ions by Zn and O atoms, respectively. Because of the smaller scattering cross section of O atoms, the intensity of O atoms is weaker than that of Zn atoms. By monitoring the change of the intensity of scattered He^+ ions by Zn atoms as a function of polar and azimuth angles, we have obtained CAICISS spectra, which should have information on the lattice polarity of the films.

B. CAICISS spectra of ZnO films

Figures 5(a) and 5(b) show experimental (solid squares) and simulated (open circles) CAICISS spectra as a function of incident angle (=90°−polar angle) from Zn- and O-plasma-preexposed ZnO films, respectively. The simulation program used is based on a three-dimensional two-atom model. Using this program, the scattering cross section of target atoms arbitrarily placed in three-dimensional space can be calculated.[24] The spectra show significantly different features for both types of samples. The measured CAICISS spectrum of the Zn-preexposed ZnO film is characterized by three dominant peaks at $\theta=24°$, 50°, and 74°. The simulated spectrum obtained for Zn-polar ZnO with the topmost surface being terminated with Zn atoms shows dominant peaks at $\theta=24°$, 50°, and 74°. Although the linewidth and intensity of the peaks in the simulated spectrum show difference from the experimental ones, the essential features of the simulated spectrum agree with the CAICISS spectrum of the Zn-preexposed ZnO film. We noted that any of the simulated CAICISS spectra for Zn-polar ZnO with the topmost surface being terminated with O atoms or O-polar ZnO with both surface terminations are far different from the CAICISS spectrum of the Zn preexposed ZnO film. In the case of O-plasma-preexposed ZnO films, four dominant peaks at $\theta=22°$, 36°, 54°, and broad peak in the range 72°–76° characterize the experimental CAICISS spectrum. The essential

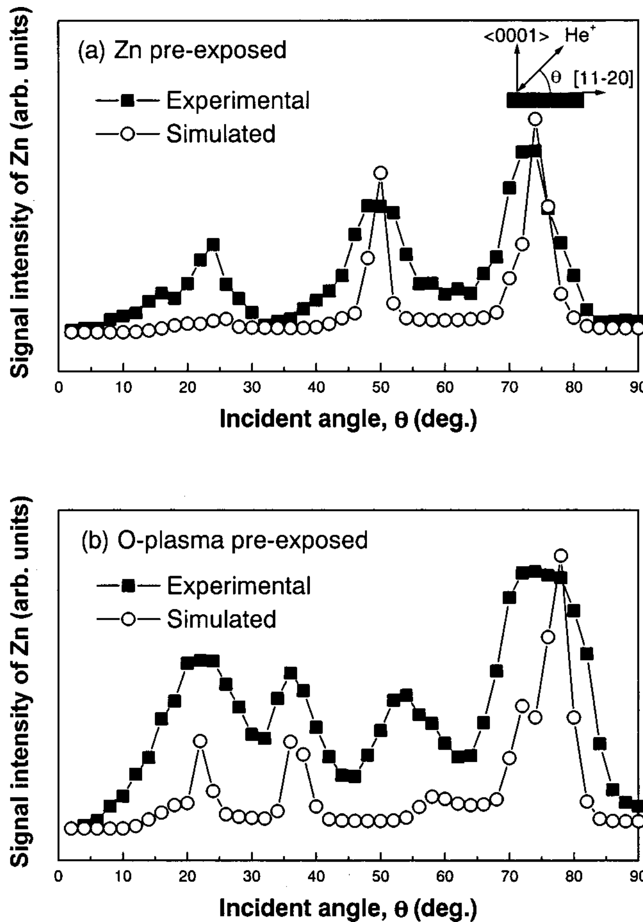

FIG. 5. Polar-angle-dependent CAICISS spectra from ZnO films with (a) Zn preexposure and (b) O-plasma preexposure. Solid squares and open circles indicate experimental and simulated spectra [Zn polar for (a) and O polar for (b)], respectively. The spectra are plotted as a function of an incident angle, where 90° minus a polar angle is an incident angle.

features of the spectrum agree with the simulated spectrum obtained for O-polar ZnO with O-atom termination, which shows dominant peaks at 22°, 36°, 58°, 72°, and 78°. We note again that none of the simulated spectra for the surface structures of Figs. 1(a), 1(c), and 1(d) can represent the experimental features better. By simply comparing Figs. 5(a) and 5(b), it is easy to see that the calculated spectrum for O-polar ZnO cannot simulate the experimental one for Zn-preexposed ZnO and that the simulated spectrum for Zn-polar ZnO is different from the measured one for O-plasma-exposed ZnO.

Let us comment on the origin of the observed discrepancy between the experimental and the simulated CAICISS spectra. First of all, the simulated spectra are calculated assuming the bulk structure of ZnO without taking surface reconstruction into account. Additionally, the scattered signal can be more affected by surface contamination when the incident angle is small. Since a Zn-terminated, Zn-polar surface is easily contaminated in ambient air before measurement, the observed discrepancy at lower incident angle can be ascribed to residual surface contamination, although the specimen was thermally cleaned at 200 °C for 30 min before the CAICISS measurements. It should be noted, however, that the same conclusions as CAICISS are obtained by CBED on the polarity of the ZnO layers as will be discussed later.

Figure 6 shows the azimuth angle dependence of the Zn signal at an incident angle of 58.5° for (a) Zn-preexposed and (b) O-plasma-preexposed samples. Figures 6(c) and 6(d) show simulated azimuth spectra for Zn-polar and O-polar ZnO with various surface terminations. The observed features in the CAICISS spectra will be discussed in Sec. VI.

V. BULK STRUCTURE ANALYSIS BY CBED

Because the polarity is a bulk property and not a surface property, CBED has been widely used to determine the polarity of a wurtzite-structure material.[25,26] Compared with CAICISS, CBED has the advantage that we can analyze several multiple layers, at the same time, such as the ZnO/GaN heterostructure. The probed region by CBED is of nanometer scale, and the symmetry of a pattern is very sensitive to strain and defects in the film. In this study, CBED experiments are performed using JEOL 2000 TEM at 100 keV with a minimum probe size of 5 nm. The CBED patterns are obtained with about a 20-nm probe for several regions per sample with the zone axis of [2-1-10]. Experimental CBED patterns from ZnO and GaN layers are compared with the simulated patterns for TEM specimen thicknesses of 10–80 nm.

Figure 7(a) shows experimental CBED patterns of an upper ZnO and a lower GaN film from a Zn preexposed sample. The arrow indicates the growth direction. The experimental CBED patterns from the upper ZnO and the lower GaN films are nearly the same. This may indicate that the polarity of the upper ZnO film is of Zn polarity because we have used MOCVD-grown Ga-polar GaN templates as substrates and the CBED patterns from GaN and ZnO are most likely very similar considering the structural similarity between ZnO and GaN. Figure 7(b) shows experimental CBED patterns of an upper ZnO and a lower GaN film from an O-plasma preexposed sample. Note that the experimental CBED patterns from the upper ZnO and lower GaN films appear opposite. This may imply that the polarity of the ZnO film is opposite to that of the underlying GaN, and hence the polarity of ZnO film is of O polar. In order to determine the polarity without ambiguity, comparisons with simulated CBED patterns from ZnO and GaN are performed. Figure 7(c) shows simulated CBED patterns from wurtzite ZnO and GaN. The simulated patterns correspond to 28- and 45-nm-thick ZnO and GaN, in which the upward directions are aligned to Zn- and Ga-polar, respectively. Comparison of the experimental and simulated CBED patterns directly indicates that the polarity of ZnO film with O-plasma preexposure is of O-polar and that of ZnO film with Zn preexposure is of Zn-polar, which agree with the CAICISS results.

VI. DISCUSSION

A. Interpretation of CAICISS spectra

In order to understand the origin of the features in the CAICISS spectra, we must know the shape of shadow cones

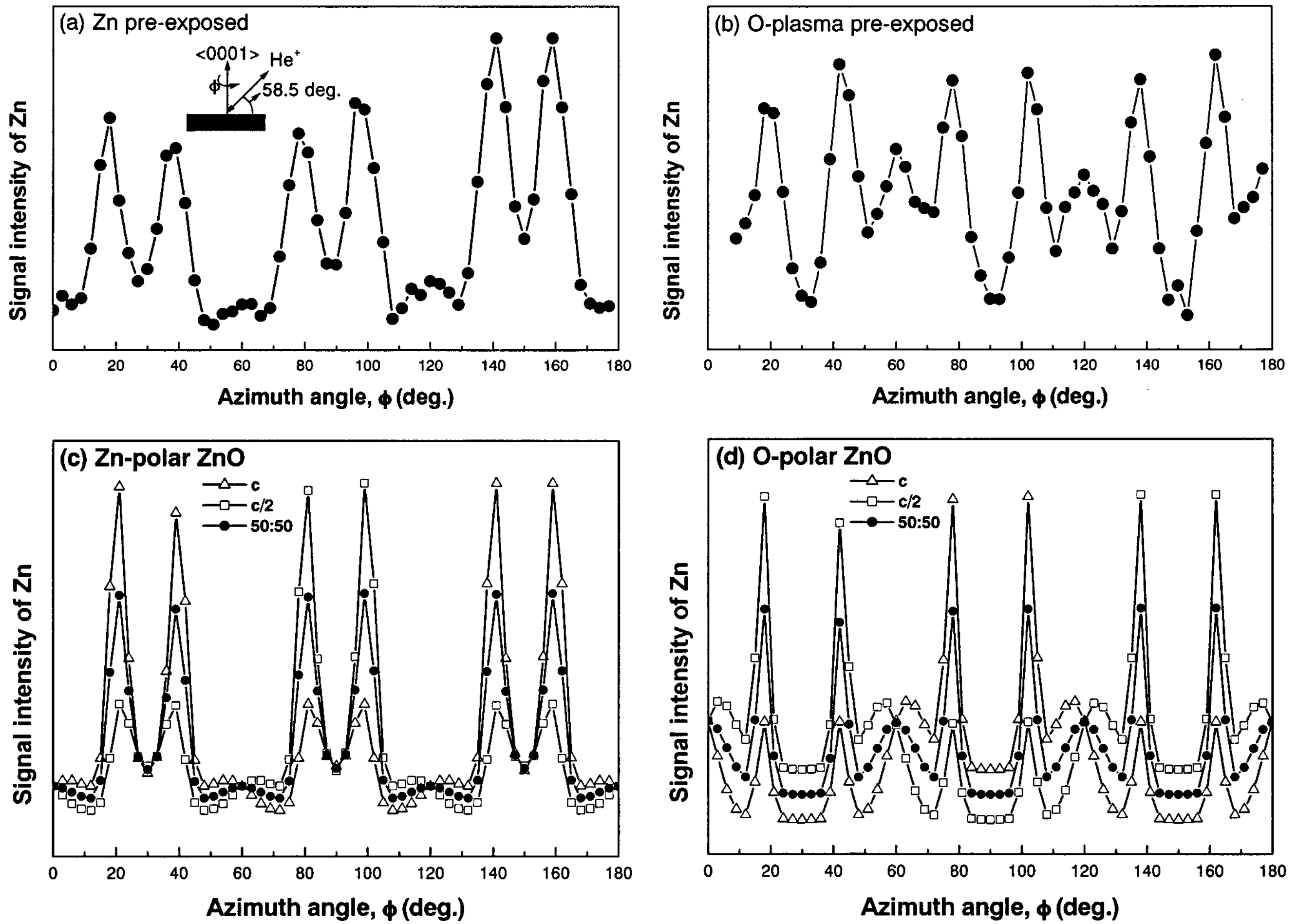

FIG. 6. Azimuth-angle-dependent CAICISS spectra from ZnO films with (a) Zn preexposure and (b) O-plasma preexposure, and (c) a simulated spectrum for Zn-polar and (d) a simulated spectrum for O-polar ZnO.

formed by Zn and O atoms. The atoms in the shadow cone cannot participate in the scattering process of the primary ions. Hence no signal will be detected at such an incidence angle. The shape of a shadow cone formed by an atom is expressed by the following formula:[27]

$$\frac{R_C}{2\sqrt{bl}} = 1.0 - 0.12\alpha + 0.01\alpha^2 \quad (\text{for } 0 \leqslant \alpha \leqslant 4.5)$$

$$= 0.924 - 0.182 \ln \alpha + 0.008\alpha$$

$$(\text{for } 4.5 \leqslant \alpha \leqslant 100). \tag{2}$$

Here R_C is the radius of the shadow cone, $b = Z_1 Z_2 e^2/E$, where Z_1 and Z_2 are, respectively, atomic numbers of the incident ion and the target atom, e is the electron charge, E is the energy of the incident ion in eV, $\alpha = 2\sqrt{bl}/a$, $a = 0.4685\ (\sqrt{Z_1} + \sqrt{Z_2})^{-2/3}$, and l is the distance behind the target atom. Figure 8 shows calculated radii of the shadow cones for Zn and O atoms formed by the incident ions at 2 kV. The shadow cone for a Zn atom has a larger radius due to the larger atomic number.

Considering the shadow cones and the structure of wurtzite ZnO, it is possible to understand the observed features in the CAICISS spectra. Figure 9 shows the schematics of shadow cones at the surfaces of Zn-polar ZnO [Figs. 9(a) and 9(b)] and O-polar ZnO [Figs. 9(c) and 9(d)] for incidence angles of 36° [Figs. 9(a) and 9(c)] and 50° [Figs. 9(b) and 9(d)]. The ZnO structure in Fig. 9 is viewed along the ⟨1-100⟩ direction. Solid circles and hatched circles represent Zn and O atoms, respectively. Larger circles and smaller circles are located on different {2-200} planes along the ⟨1-100⟩ direction. Here it should be noted that interplane spacing of adjacent {2-200} planes in bulk ZnO is 0.141 nm, which is much larger than the radius of the shadow cone of a Zn atom. Note that the radius of the shadow cone of a Zn atom even behind a 1-nm depth, for example, is 0.132 nm as shown in Fig. 8. Therefore, the atoms on different {2-200} planes do not shadow each other and hence consideration of the shadow cones for atoms on the same {2-200} planes is enough.

In the case of a Zn-polar surface, Zn atoms on the second and fifth layers are shadowed respectively by O atoms on the second and fourth layers at an ion incident angle of 36° [Fig. 9(a)]. Therefore, when the incident angle is 36°, the signals scattered by Zn atoms will not be observed. At an incident angle of 50° [Fig. 9(b)], the signals due to scattering by Zn atoms will be detected, since Zn atoms on the third layer are not shadowed by O atoms on the second layer and Zn atoms

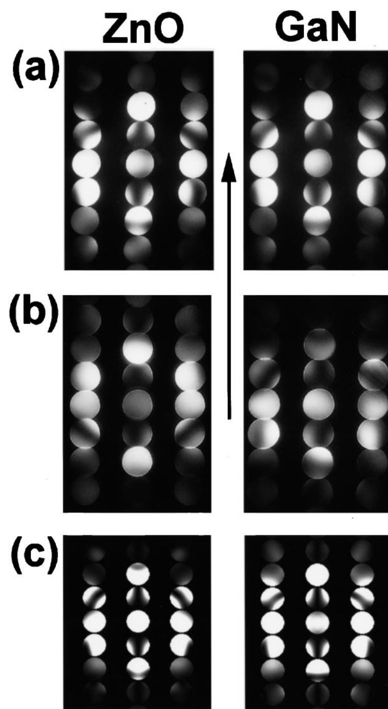

FIG. 7. Experimental CBED patterns of the upper ZnO and lower GaN films from (a) Zn-preexposed sample and (b) O-plasma-preexposed sample, and (c) simulated CBED patterns of wurtzite ZnO and GaN with the zone axis of the [2-1-10] direction. The arrow indicates the growth direction. The simulated patterns correspond to 28 and 45 nm thicknesses of ZnO and GaN, respectively, in which the upward directions are aligned to Zn and Ga polarities.

on the fifth layer are not shadowed by O atoms on the fourth layer. Furthermore, the focusing effect would occur at this incidence angle, because those atoms are located at the edge of the shadow cones formed by Zn atoms on the first layer. The flux of scattered ions will be concentrated at this incidence angle, which results in an enhancement of the signal intensity due to scattering by Zn atoms on the fifth layer. Therefore, a strong peak should be observed at an incidence angle of 50° in the CAICISS spectrum of a Zn-polar ZnO surface. This is the case as is observed in Fig. 5(a). On the other hand, in the case of an O-polar surface [Fig. 9(c)], Zn atoms in the fourth and sixth layers are not shadowed by O atoms in the first and third layers at an ion incident angle of

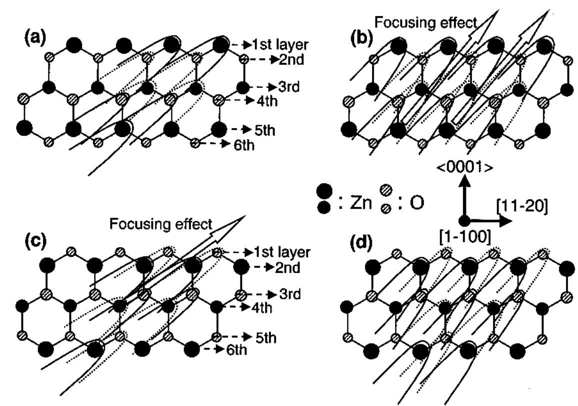

FIG. 9. Schematic illustration for shadowing cones for (a) Zn-polar with Zn-atom termination for an incident angle of 36°, (b) Zn-polar with Zn-atom termination for an incident angle of 50°, (c) O-polar with O-atom termination for an incident angle of 36°, and (d) O-polar with O-atom termination for an incident angle of 50°.

36°. Additionally, the focusing effect will occur because Zn atoms in the fourth layer are located at the edge of the shadow cones formed by O atoms in the first layer, which will enhance the strong signal due to scattering by Zn atoms in the fourth layer. At an incident angle of 50° [Fig. 9(d)], Zn atoms in the fourth and sixth layers are shadowed by O atoms in the first and third layers, respectively. Therefore, when the incident angle is 50°, the signal scattered by Zn atoms will be weak and difficult to be observed from the O-polar ZnO surface. This will explain the observed features in Fig. 5(b).

There are two other surface structures as described in Fig. 1: O-polar with a Zn-atom termination and Zn-polar with an O-atom termination. When finishing the growth, the Zn shutter was closed and simultaneously O plasma was turned off. However, the inside of the growth chamber was still under oxygen ambient at least for a few minutes until the residual oxygen gas was fully evacuated. Furthermore, the samples were exposed to air prior to the CAICISS measurements, although the samples were thermally cleaned in the CAICISS chamber just before measurement. Therefore, the topmost surface of the ZnO samples might have been more or less terminated by O atoms resulting in either Zn-polar ZnO with O termination instead of O-polar ZnO with O termination. Consequently, our interest is how to distinguish be-

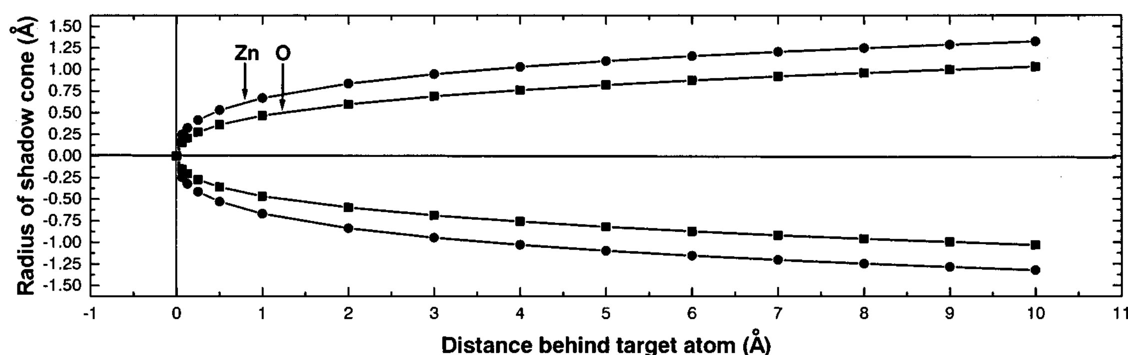

FIG. 8. Calculated shadow cones for Zn and O atoms formed by 2-kV He^+ ions.

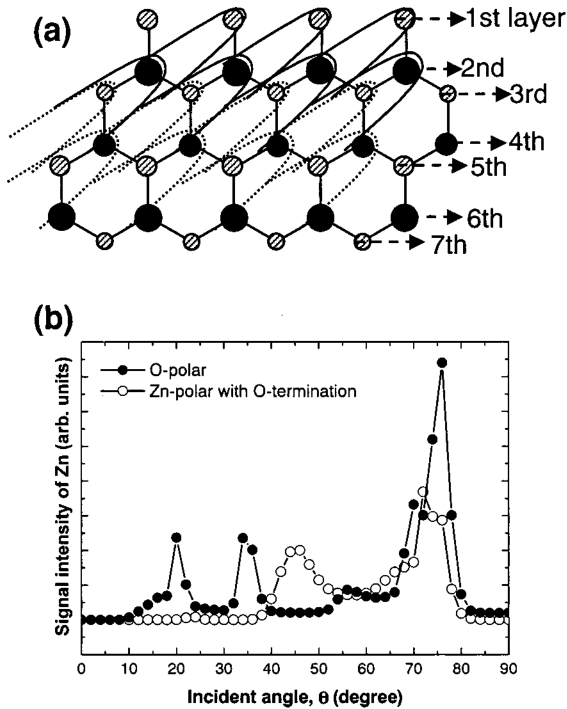

FIG. 10. Schematic illustration for showing cones for (a) Zn-polar with O-atom termination for an incident angle of 36°, and (b) simulated CAICISS spectra for O-polar with O-atom termination (solid circle) and Zn-polar with O-atom termination (open circle).

tween the two cases: (1) O-polar with O-atom termination and (2) Zn-polar with O-atom termination. Figure 10(a) shows schematics of the shadow cones for an O-atom-terminated Zn-polar surface at an incident angle of 36°. Since Zn atoms in the second and fourth layers are shadowed by O atoms in the first and third layers in this case, no signal will be expected at this incidence angle as is shown in the simulated CAICISS spectrum for Zn-polar ZnO with O termination. On the other hand, as illustrated in Fig. 9(c), a strong signal is expected from a O-atom-terminated O-polar surface due to the focusing effect, which should give rise to a strong peak at an incidence angle of 36° in the simulated CAICISS spectrum. The simulated CAICISS spectra for these two cases are shown in Fig. 10(b). By comparing the simulated CAICISS spectra shown in Fig. 10(b) with the experimental CAICISS spectrum for the O-plasma-preexposed ZnO sample shown in Fig. 5(b), it is readily concluded that the surface structure of the sample is of O-atom-terminated O-polar ZnO not Zn-polar with O-atom termination. These results would imply that adsorbed oxygen on as-grown Zn-polar surface was effectively removed by the treatments prior to measurement.

The CAICISS signals for other incident angles can be understood similarly in terms of the shadowing and focusing effects. Although all the features support the conclusions that the ZnO layers grown on an O-plasma-treated GaN template grew as O-polar ZnO with the topmost surface being oxygen atoms, while the Zn preexposure on a GaN template helped grow Zn-polar ZnO layers, there still remain discrepancies between the measured CAICISS spectra and the simulated ones. Let us comment on the origin of these discrepancies. When simulating the CAICISS spectra, we have assumed that the crystal structure of ZnO at around the surface does not undergo rearrangement of atoms. Multiple scattering was not taken into account. It is likely that those factors may have evoked the observed discrepancies between the simulated and experimental CAICISS spectra. Nevertheless, we would like to stress again that the essential features of the observed CAICISS spectra are well simulated based on the models that Zn-polar ZnO is grown on Zn-preexposed GaN, while O-polar ZnO is grown on O-plasma-preexposed GaN.

Now we discuss the azimuth angle dependence of the CAICISS spectra. The azimuth angle dependence at a fixed incident angle reveals the terminating topmost plane in addition to the polarity of a film.[24] The stable termination of a wurtzite-structure (0001) surface is either c or, $c/2$ plane, where c is the unit cell length along the [0001] direction. Here it should be noted that the surface terminated at c or $c/2$ plane has the same polarity and hence such a termination cannot be distinguished in the incidence angle dependence of CAICISS spectra. Figures 6(c) and 6(d) show simulated azimuth spectra for Zn- and O-polar surfaces terminating at c or $c/2$ plane and for mixtures of c and $c/2$ planes at a ratio of 50:50. Although the main peak and dip positions are the same for the three cases, the relative peak intensity ratios and the positions of the small peaks at around 60° and 120° show some difference. Careful comparison between the experimental CAICISS spectra and the simulated spectra reveals that the experimental CAICISS spectra for a Zn-preexposed ZnO layer and O-plasma-preexposed ZnO layer are best simulated by assuming that the topmost surface of ZnO is mixed with c and $c/2$ steps at a ratio of 50:50, respectively, for both Zn-and O-polar ZnO. It is likely that the agreement between the experimental spectra and the simulated one would be more improved if the mixture ratio of the two steps were adjusted. However, in view of the S/N ratio, a more detailed analysis will be meaningless.

B. Polarity control by interface engineering

The CAICISS and CBED analyses reveal that we can selectively grow both Zn- and O-polar ZnO films by P-MBE even on Ga-polar GaN templates by engineering the interface. Let us discuss the mechanism for inversion of the polarity in the ZnO/GaN heterostructure. The growth of O-polar (anion-polar) ZnO on Ga-polar (cation-polar) becomes possible by the formation of the Ga_2O_3 interface layer with a monoclinic structure in between the GaN and ZnO films. By definition, the polarity is caused by a lack of inversion center as cases for wurtzite-structure crystals. If a crystalline layer whose crystal structure has inversion symmetry is deposited on a surface of a Ga-polar GaN surface, for example, it would be possible to interrupt the propagation of lattice polarity to the overlayer on the interface layer to invert the polarity. The monoclinic Ga_2O_3 interface layer has a center of symmetry, since the space group of Ga_2O_3 is $C2/m$. Hence it becomes possible to interrupt the propagation of the lattice polarity from GaN to ZnO by inserting a

monoclinic Ga_2O_3 interface layer in between to convert the lattice polarity. We would like to stress again that the present results suggest a generalized method to control the lattice polarity of films by inserting an interface layer with a center of symmetry: thereby, the conversion of lattice polarity becomes possible. It should be noted that the proposed method for controlling lattice polarity is more general than any of the previous method using inverted domains.[25,26]

C. Comparison of the structural properties of ZnO films with different polarities

Let us compare the crystal quality of the Zn-preexposed films with those of the O-plasma-preexposed ZnO films. The full width at half maximum (FWHM) values of symmetric (0001) and asymmetric (10-10) x-ray rocking curves for an O-plasma-preexposed ZnO (Zn-preexposed ZnO) film were 0.19° (0.11°) for symmetric and 0.28° (0.21°) for asymmetric diffractions. The total dislocation densities evaluated by TEM and HRXRD ranged in the middle of $10^9/cm^2$ for O-plasma-preexposed ZnO films and in low $10^9/cm^2$ for Zn-preexposed ZnO films. The observed degraded crystal quality in O-plasma-preexposed ZnO layers can be ascribed to the presence of the monoclinic Ga_2O_3 interface layer at the ZnO/GaN interface. It should be noted again that a prolonged exposure of O plasma changed the monoclinic Ga_2O_3 into amorphous. Furthermore, we noted that the TEM diffraction spots from the Ga_2O_3 layer are diffusive, indicative of degraded crystallinity. Additionally, the lattice misfits with both ZnO and GaN are much larger than that for the ZnO/GaN. All of those would contribute to the degradation of the ZnO overlayers with O polarity.

VII. CONCLUSIONS

A general method for polarity control has been proposed with the demonstration of the growth of Zn-polar (cation-polar) and O-polar (anion-polar) ZnO films on Ga-polar (cation-polar) GaN templates by engineering the interface. The key is inserting an interface layer that has a center of symmetry because the polarity comes from the lack of the center of symmetry. By inserting a single-crystalline Ga_2O_3 layer, which has a center of symmetry, in between ZnO and Ga-polar GaN, the ZnO film was grown as O polar, while Zn-polar ZnO film without forming an interface layer. There was no formation of planar and faceted inversion domain boundaries inverting the polarity. The orientation relationship and plausible in-plane lattice matching for $ZnO/Ga_2O_3/GaN$ were determined. Induced larger lattice misfit by the Ga_2O_3 layer resulted in degradation of the crystal quality of ZnO films. The features of CAICISS spectra were analyzed by considering shadow cones of Zn and O formed by incident ions and shadowing and focusing effects.

ACKNOWLEDGMENTS

S.-K.H. would like to thank the International Communications Foundation (ICF) for its financial support.

*Corresponding author. Present address: Faculty of Engineering, Brown University, 182 Hope St., Box D, Providence, RI 02912. FAX: 401 863 9107. Electronic address: soon-ku_hong@brown.edu

[1] D. M. Bagnall, Y. F. Chen, Z. Zhu, T. Yao, S. Koyama, M. Y. Shen, and T. Goto, Appl. Phys. Lett. **70**, 2230 (1997).
[2] Z. K. Tang, G. K. L. Wong, P. Yu, M. Kawasaki, A. Ohotomo, H. Koinuma, and Y. Segawa, Appl. Phys. Lett. **72**, 3270 (1998).
[3] D. M. Bagnall, Y. F. Chen, Z. Zhu, T. Yao, M. Y. Shen, and T. Goto, Appl. Phys. Lett. **73**, 1038 (1998).
[4] Y. Chen, D. M. Bagnall, Z. Zhu, T. Sekiuchi, K. T. Park, K. Hiraga, T. Yao, S. Koyama, M. Y. Shen, and T. Goto, J. Cryst. Growth **181**, 165 (1997).
[5] Y. Chen, D. M. Bagnall, H. J. Ko, K. T. Park, K. Hiraga, Z. Zhu, and T. Yao, J. Appl. Phys. **84**, 3912 (1998).
[6] H. J. Ko, Y. F. Chen, T. Yao, K. Miyajima, A. Yamamoto, and T. Goto, Appl. Phys. Lett. **77**, 537 (2000).
[7] V. Kirilyuk, A. R. A. Zauner, P. C. M. Christianen, J. L. Weyher, P. R. Hageman, and P. K. Larsen, Appl. Phys. Lett. **76**, 2355 (2000).
[8] R. Dimitrov, M. Murphy, J. Smart, W. Schaff, J. R. Shealy, L. F. Eastman, O. Ambacher, and M. Stutzmann, J. Appl. Phys. **87**, 3375 (2000).
[9] L. K. Li, M. J. Jurkovic, W. I. Wang, J. M. Van Hove, and P. P. Chow, Appl. Phys. Lett. **76**, 1740 (2000).
[10] M. Sumiya, K. Yoshimura, K. Ohtsuka, and S. Fuke, Appl. Phys. Lett. **76**, 2098 (2000).
[11] H. Weinisch, V. Kirchner, Y. Chen, S. K. Hong, H. J. Ko, and T. Yao (unpublished).
[12] S. K. Hong, T. Hanada, H. J. Ko, Y. Chen, T. Yao, D. Imai, K. Araki, and M. Shinohara, Appl. Phys. Lett. **77**, 3571 (2000).
[13] S. K. Hong, H. J. Ko, Y. Chen, T. Hanada, and T. Yao, Appl. Surf. Sci. **159/160**, 441 (2000).
[14] H. J. Ko, Y. Chen, S. K. Hong, and T. Yao, J. Cryst. Growth **209**, 816 (2000).
[15] A. Ohtake, S. Miwa, L. H. Kuo, T. Yasuda, K. Kimura, C. Jin, and T. Yao, J. Cryst. Growth **164/185**, 163 (1998).
[16] R. D. Vispute, V. Talynsky, S. Choopun, R. P. Sharma, T. Venkatesan, M. He, X. Tang, J. B. Halpern, M. G. Spencer, Y. X. Li, L. G. Salamanca-Riba, A. A. Iliadis, and K. A. Jones, Appl. Phys. Lett. **73**, 348 (1998).
[17] S. K. Hong, H. J. Ko, Y. Chen, T. Hanada, and T. Yao, J. Vac. Sci. Technol. B **18**, 2313 (2000).
[18] T. Zheleva, K. Jagannadham, and J. Narayan, J. Appl. Phys. **75**, 860 (1994).
[19] T. Ohinishi, A. Phtomo, M. Kawasaki, K. Takahashi, M. Yoshimoto, and H. Koinuma, Appl. Phys. Lett. **72**, 824 (1998).
[20] S. Fuke, H. Tesshigawara, K. Kuwahara, Y. Takano, T. Ito, M. Yanagihara, and K. Ohtsuka, J. Appl. Phys. **83**, 764 (1998).
[21] S. Sonoda, S. Shimizu, Y. Suzuki, K. Balakrishnan, J. Shirakashi, and H. Okumura, Jpn. J. Appl. Phys., Part 2 **39**, L73 (2000).
[22] X. Q. Shen, T. Ide, S. H. Cho, M. Shimizu, S. Hara, H. Okumura, S. Sonoda, and S. Shimizu, J. Cryst. Growth **218**, 155 (2000).

[23] M. Aono and R. Souda, Jpn. J. Appl. Phys., Part 1 **24**, 1249 (1985).
[24] O. Ishiyama, T. Nishihara, M. Shinohara, F. Ohtani, S. Nishino, and J. Saraie, Appl. Phys. Lett. **70**, 2105 (1997).
[25] V. Ramachandran, R. M. Feenstra, W. L. Samey, L. Salamanca-Riba, J. E. Northrup, L. T. Romano, and D. W. Greve, Appl. Phys. Lett. **75**, 808 (1999).
[26] L. T. Romano, J. E. Northrup, A. J. Ptak, and T. H. Myers, Appl. Phys. Lett. **77**, 2479 (2000).
[27] O. S. Oen, Surf. Sci. **131**, L407 (1983).